The Astrophysical Journal Supplement Series, 154:124–129, 2004 September

SPITZER OBSERVATIONS OF MAMBO GALAXIES: WEEDING OUT ACTIVE NUCLEI IN STARBURSTING PROTOELLIPTICALS

R. J. Ivison,[1,2] T. R. Greve,[2] S. Serjeant,[3] F. Bertoldi,[4] E. Egami,[5] A. M. J. Mortier,[3] A. Alonso-Herrero,[5] P. Barmby,[6] L. Bei,[5] H. Dole,[5] C. W. Engelbracht,[5] G. G. Fazio,[6] D. T. Frayer,[7] K. D. Gordon,[5] D. C. Hines,[5] J.-S. Huang,[6] E. Le Floc'h,[5] K. A. Misselt,[5] S. Miyazaki,[8] J. E. Morrison,[5] C. Papovich,[5] P. G. Pérez-González,[5] M. J. Rieke,[5] G. H. Rieke,[5] J. Rigby,[5] D. Rigopoulou,[9] I. Smail,[10] G. Wilson,[7] and S. P. Willner[6]

Received 2004 March 26; accepted 2004 May 29

ABSTRACT

We present 3.6–24 μm *Spitzer* observations of an unbiased sample of nine luminous, dusty galaxies selected at 1200 μm by MAMBO on the IRAM 30 m telescope, a population akin to the well-known submillimeter or SCUBA galaxies (hereafter SMGs). Owing to the coarse resolution of submillimeter/millimeter cameras, SMGs have traditionally been difficult to identify at other wavelengths. We compare our multiwavelength catalogs to show that the overlap between 24 and 1200 μm must be close to complete at these flux levels. We find that all (4/4) of the most secure $\geq$4 σ SMGs have $\geq$4 σ counterparts at 1.4 GHz, while the fraction drops to 7/9 using all $\geq$3 σ SMGs. We show that combining mid-infrared (MIR) and marginal ($\geq$3 σ) radio detections provides plausible identifications in the remaining cases, enabling us to identify the complete sample. Accretion onto an obscured central engine is betrayed by the shape of the MIR continuum emission for several sources, confirming *Spitzer*'s potential to weed out active galaxies. We demonstrate the power of an $S_{24\ \mu m}/S_{8\ \mu m}$ versus $S_{8\ \mu m}/S_{4.5\ \mu m}$ color-color plot as a diagnostic for this purpose. However, we conclude that the majority ($\sim$75%) of SMGs have rest-frame mid/far-IR spectral energy distributions commensurate with obscured starbursts. Sensitive 24 μm observations are clearly a useful route to identify and characterize reliable counterparts to high-redshift far-IR–bright galaxies, complementing what is possible via deep radio imaging.

Subject headings: galaxies: evolution — galaxies: formation — galaxies: starburst

Online material: color figures

1. INTRODUCTION

Major progress has been made in our understanding of galaxy formation and evolution since the discovery of a significant population of submillimeter/millimeter-bright, dusty galaxies. The first handful of galaxies, discovered behind lensing clusters (Smailet al. 1997) and in the Hubble Deep Field (Hughes et al. 1998), revealed the diversity of the population. SCUBA (Holland et al. 1999), the innovative camera with which SMGs were first seen, was commissioned on the James Clerk Maxwell Telescope during 1996–1997. Since then, the 117 bolometer, 1200 μm MAMBO camera (Bertoldi et al. 2000) has been installed on the IRAM 30 m telescope in Spain. Surveys at 1200 μm are sensitive to the same dusty galaxies as SCUBA, yet have a selection function that potentially stretches to higher redshifts and is sensitive to lower dust temperatures (Eales et al. 2003; Blain et al. 2004b).

A moderate fraction of SMGs can be pinpointed by their μJy-level emission at 1.4 GHz (Ivison et al. 2002), allowing us to identify their counterparts in other wave bands. However, up to 30% of the population remain undetected in the radio wave band in even the deepest maps and the properties of these galaxies remain a mystery. Those SMGs that can be localized through their radio emission are usually found in the optical/IR wave bands to be faint, morphologically complex systems, often comprising red galaxies with bluer companions, as expected for a distant, dust-reddened, interacting star-forming population (Ivison et al. 2002; Smail et al. 2002; Webb et al. 2003). Recent advances in their study include the measurement of the redshift distribution of radio-detected SMGs (Chapman et al. 2003), the resolution of most of the submillimeter background by exploiting gravitational lensing (Blain et al. 1999; Cowie et al. 2002), the identification of X-ray emission from a significant fraction of the population (Alexander et al. 2003), the detection (via broad CO lines) of colossal quantities ($\sim 10^{11}\ M_{\odot}$) of molecular gas (Frayer et al. 1998; Neri et al. 2003; T. R. Greve et al. 2004, in preparation), and the first indications of the strong clustering expected for such massive galaxies (Blain et al. 2004a). These discoveries underline the importance of studying the far-IR–luminous SMGs to our understanding of the formation of massive galaxies at high redshifts.

For local IR-luminous galaxies, MIR data from the *Infrared Space Observatory* (*ISO*) were used to develop a number of useful diagnostics to differentiate between those powered

[1] Astronomy Technology Centre, Royal Observatory, Blackford Hill, Edinburgh EH9 3HJ, UK.
[2] Institute for Astronomy, University of Edinburgh, Blackford Hill, Edinburgh EH9 3HJ, UK.
[3] Centre for Astrophysics and Planetary Science, University of Kent, Canterbury, Kent CT2 7NR, UK.
[4] Max-Planck-Institut für Radioastronomie, Auf dem Hügel 69, 53121 Bonn, Germany.
[5] Steward Observatory, University of Arizona, 933 North Cherry Avenue, Tuscon, AZ 85721.
[6] Harvard-Smithsonian Center for Astrophysics, 60 Garden Street, Cambridge, MA 02138.
[7] *Spitzer* Science Center, California Institute of Technology, 1200 East California Boulevard, Pasadena, CA 91125.
[8] Subaru Telescope, National Astronomical Observatory of Japan, 650 North Aohoku Place, Hilo, HI 96720.
[9] Astrophysics, Denys Wilson Building, Keble Road, Oxford OX1 3RH, UK.
[10] Institute for Computational Cosmology, University of Durham, South Road, Durham DH1 3LE, UK.

predominantly by starbursts and by active galactic nuclei (AGNs; Genzel & Cesarsky 2000). *ISO* was sensitive to only the most luminous SMGs, so efforts to assess the preponderance of AGNs in SMGs have so far been reliant on UV/optical spectroscopy, radio observations, and the aforementioned X-ray imaging, often with ambiguous results. The fraction of distant, far-IR–luminous galaxies with an energetically dominant AGN remains poorly determined, although it is expected to be small: even SMGs with unambiguous AGN characteristics (Ivison et al. 1998) are thought to have a major starburst contribution to their bolometric luminosities (Frayer et al. 1998; Genzel et al. 2003). This finding has been echoed in studies of distant quasars and radio galaxies: far-IR–luminous examples are found to be gas-rich and their submillimeter emission is often resolved, as expected if their power originates in large part from stars (Omont et al. 1996; Papadopoulos et al. 2000; Stevens et al. 2003).

In this paper, we use MIR continuum imaging of nine MAMBO-selected SMGs in the Lockman Hole to investigate the use of MIR data to identify the counterparts at other wavelengths of this population and demonstrate the power of MIR data for determining the likely power source (AGN or starburst) in these galaxies.

2. MAMBO GALAXIES AND THE DIAGNOSTIC POTENTIAL OF *SPITZER*

Greve et al. (2004) reported the results of a deep unbiased MAMBO survey of the Lockman Hole, a region mapped earlier by the SCUBA 8 mJy survey (Scott et al. 2002). This region was selected for reasons that included its low Galactic cirrus emission and the availability of high-quality complementary data. Not surprisingly, the same region was selected for some of the earliest imaging with *Spitzer* (Werner et al. 2004). The data exploited herein were obtained using the Infrared Array Camera (IRAC; Fazio et al. 2004) and Multiband Imaging Photometer for *Spitzer* (MIPS; Rieke et al. 2004), reaching noise levels of $\sigma = 0.8$, 0.8, 2.8, 1.7, and 30 μJy at 3.6, 4.5, 5.8, 8.0, and 24 μm with absolute calibration accurate to $\pm$10%. These compare with 5 σ confusion limits (20 beams per source) of $\sim$1.0, 1.2, and 56 μJy at 3.6, 8.0, and 24 μm. The images cover a $5' \times 5'$ region, centered near the SMG LE 850.01 (Table 1). Data were reduced using standard *Spitzer* data analysis tools, as described by Le Floc'h et al. (2004) and Huang et al. (2004).

Our analysis also makes use of deep imaging from the Subaru 8 m telescope (R, 3 $\sigma \sim 27.0$, Vega, 2″ radius aperture), *XMM-Newton* (0.5–10 keV, 3 $\sigma \sim 5 \times 10^{-16}$ ergs s^{-1} cm^{-2}) and the Very Large Array (1.4 GHz, 3 $\sigma \sim$15 μJy beam^{-1}) (Ivison et al. 2002).

The 1200 μm sample includes nine $\geq$3 σ MAMBO sources within the region covered by IRAC/MIPS. Four are detected at $\geq$4 σ, all of which should be secure. The other five are $\geq$3 σ detections, of which up to two may be the result of noise fluctuations, Eddington bias, or confusion. Greve et al. (2004) performed Monte Carlo simulations to determine the reliability of their source catalog. We list the flux densities, significance, and positions for all nine sources in Table 1 and note that the positions are accurate to $\pm$4″ (95% confidence).

Figure 1 shows the spectral energy distributions (SEDs) of typical local starburst- and AGN-dominated IR-luminous galaxies and several SMGs with well-sampled UV-radio spectra. It is worth reviewing the emission mechanisms operating across the observable wavelength range: where our adopted sample was selected, at 1200 μm (rest-frame far-IR), we are sensitive to cold dust ($\sim$40 K) created in copious quantities by supernovae (SNe; Dunne et al. 2003), which reradiates energy absorbed in the UV from hot, young stars. In the radio, at 1.4 GHz, we are again sensitive to SNe (and hence to recent star formation) via synchrotron radiation from relativistic electrons. Contamination via radio-loud AGNs is possible and at μJy flux levels is virtually impossible to distinguish from pure SNe-related emission. We are also sensitive to AGNs via X-ray emission from accretion disks and their associated coronae, although determining the origin of the X-rays is not trivial and heavily obscured AGNs can evade detection altogether (Alexander et al. 2003). At the shortest IR wavelengths accessible to *Spitzer* (3.6–8.0 μm), we are provided, via photospheric emission from stars, with a relatively unobscured measure of stellar luminosity, possibly even of stellar mass in more evolved systems out to $z > 2$. At 24 μm (rest-frame $\sim$7 μm for a galaxy at $z \sim 2$–3) we are sensitive to emission from $\sim$500 K dust in the circumnuclear torus of AGNs, and to the warmest dust in starbursts.

TABLE 1

CATALOG OF MAMBO GALAXIES IN THE *Spitzer* EARLY RELEASE OBSERVATIONS REGION

Source	$S_{1200\ \mu m}$ (mJy)	$S_{850\ \mu m}$ (mJy)[a]	$S_{24\ \mu m}$ (μJy)	$S_{8.0\ \mu m}$ (μJy)	$S_{5.8\ \mu m}$ (μJy)	$S_{4.5\ \mu m}$ (μJy)	$S_{3.6\ \mu m}$ (μJy)	$S_{1.4\ GHz}$ (μJy)	Comment
MM J105204.1+572658	3.6 ± 0.6	9.5 ± 2.8	249 ± 31	18.6 ± 1.9	27.6 ± 3.3	20.2 ± 2.1	15.2 ± 1.6	36 ± 5	*a*; LE 850.14
	...	...	...	18.5 ± 1.9	22.2 ± 3.0	14.7 ± 1.5	9.8 ± 1.0	72 ± 8	*b*
MM J105201.3+572448	3.4 ± 0.6	10.5 ± 1.6	193 ± 31	10.2 ± 1.7	11.8 ± 2.8	8.2 ± 0.9	3.8 ± 0.8	73 ± 8	LE 850.01
MM J105155.4+572310	3.3 ± 0.8	4.5 ± 1.3	125 ± 32	26.4 ± 2.7	19.9 ± 2.8	5.8 ± 0.8	6.1 ± 0.8	47 ± 5	LE 850.18
MM J105200.2+572425	2.4 ± 0.6	5.1 ± 1.3	534 ± 55	112 ± 12	79.0 ± 8.0	72.6 ± 7.3	72.0 ± 7.2	<15	*a*; $z = 0.97$, LE 850.08
	...	...	282 ± 30	89.5 ± 9.0	37.2 ± 3.8	22.3 ± 2.3	17.1 ± 1.8	80 ± 8	*b*
	...	...	162 ± 30	17.8 ± 1.8	17.2 ± 2.8	20.7 ± 2.1	26.7 ± 2.7	22 ± 6	*c*
MM J105157.6+572800	2.2 ± 0.6	<11	121 ± 30	24.5 ± 2.5	35.7 ± 3.8	29.8 ± 3.0	44.5 ± 4.5	21 ± 6	...
MM J105207.2+572558	1.7 ± 0.5	<12	<90	15.0 ± 1.7	14.5 ± 2.8	17.3 ± 1.8	12.8 ± 1.3	23 ± 6	...
MM J105203.6+572612[b]	1.7 ± 0.5	<10	166 ± 30	12.1 ± 1.7	15.8 ± 2.8	12.0 ± 1.2	7.9 ± 0.8	19 ± 6	...
MM J105216.0+572506	1.6 ± 0.5	6.7 ± 2.1	578 ± 59	...	...	...	...	48 ± 5	LE 850.29
MM J105148.5+572408	2.1 ± 0.7	<7.8	211 ± 30	16.7 ± 1.7	16.8 ± 2.8	13.4 ± 1.4	11.9 ± 1.2	29 ± 6	...

NOTE.—Italics signify sources for which robust counterparts have been identified via radio imaging; bold type indicates a robust identification made possible by the MIR data.

[a] We quote either a detection or a 3 σ limit based on the 850 μm noise measured in a 2.6 arcmin^2 region centered on the millimeter source.

[b] The source lies between LE 850.04 and LE 850.14; in the SCUBA map it would thus have been affected by the off beams of both, hence its lack of detection at 850 μm.

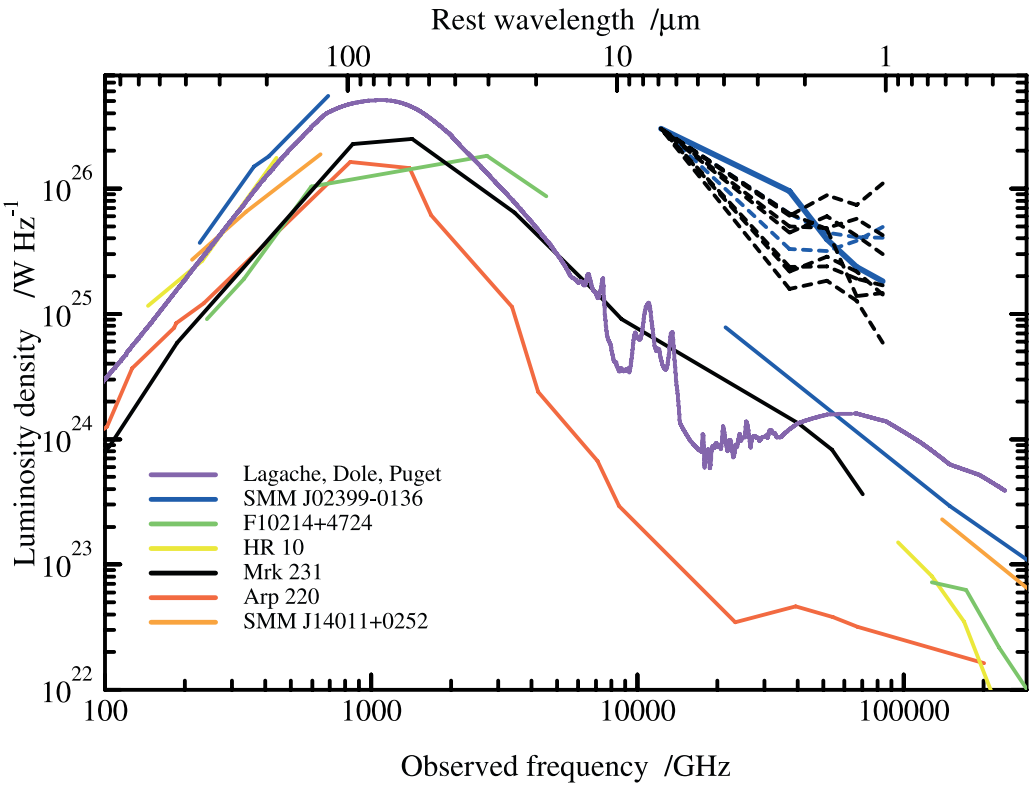

FIG. 1.—Rest-frame SEDs of well-known dusty, luminous galaxies (see Ivison et al. 2000) and the 10^{13} $L_{\odot}$ synthetic starburst SED from Lagache et al. (2003). MIR SEDs for the MAMBO galaxies in our sample are shown as dashed lines (vertically offset for clarity), normalized to give identical 24 μm luminosity densities and arbitrarily assuming a source redshift of $z = 2.5$. We distinguish the three components of MM J105200.2+572421.9 (*a*, *b*, *c*) by plotting them in blue, with a solid line representing the power-law active component *b*.

Do our *Spitzer* observations provide sufficient sensitivity to detect dust-enshrouded starbursts and AGNs in the distant universe? In Figure 1, we illustrate the SEDs of well-studied dusty, luminous galaxies and models (AGNs and starbursts). These demonstrate the range of rest-frame MIR luminosities for these systems, and we select Arp 220 and Mrk 231 to represent extremes of the starburst- and AGN-dominated subclasses. Figure 2 shows that even with its steep MIR spectrum ($\alpha = -2.9$, where $F_{\nu} \propto \nu^{\alpha}$), Arp 220 would be detected at 3.6 and 24 μm out to $z \gtrsim 1$. Mrk 231, its MIR emission boosted an order of magnitude higher than Arp 220 by its AGN, would be detected out to $z \gtrsim 3$ at 24 μm.

The diagnostic power of the near- and MIR bands (the ability to discriminate between starbursts with and without buried, active nuclei) arises from the different physical regimes and spectral features probed across the MIR wave band (Rigopoulou et al. 2002). A steeper slope between rest-frame $\sim$3–10 μm is more apparent for starbursts than for AGN-dominated galaxies. The latter, typified by Mrk 231 and SMM J02399− 0136 (Fig. 1), have power-law spectra covering rest-frame $\sim$0.2–10 μm (Ivison et al. 1998). In contrast, the SED of a starburst such as Arp 220 has a flatter region between 1 and 4 μm. Thus, for MAMBO galaxies at $z \sim 2$–3 (assuming the same median redshift as for SCUBA galaxies; Chapman et al. 2003) the key spectral indices are available in the 3.6–24 μm bands covered by IRAC and MIPS. Figure 3, an $S_{24\,\mu\mathrm{m}}/S_{8\,\mu\mathrm{m}}$ versus $S_{8\,\mu\mathrm{m}}/S_{4.5\,\mu\mathrm{m}}$ color-color plot, shows the tracks of Arp 220 and Mrk 231 as they are moved from the local universe to $z \gg 1$, as well as the track of a synthetic 10^{13} $L_{\odot}$ starburst from Lagache et al. (2003). We can see immediately that the starburst and AGN populations are well separated, and that this plot has strong diagnostic potential: we can define regions where starburst and active galaxies are likely to lie at $z = 1$–3 and hence use this to classify our SMGs.

3. MIR COUNTERPARTS TO MAMBO GALAXIES

We search for radio and MIR counterparts to the MAMBO sources within their nominal error circles (illustrated in Fig. 4 [Plate 1]). We find that all of the four most secure ≥ 4 σ MAMBO sources have robust radio counterparts at 1.4 GHz (as defined by Ivison et al. 2002). This drops slightly to 7/9 robust radio counterparts using all ≥ 3 σ MAMBO sources, somewhat higher than the 18/42 detection rate[11] reported by Dannerbauer et al. (2004). The remaining two have tentative radio identifications at ≥ 3 σ, but these are not significant enough to be reliable. If instead we had used the 24 μm *Spitzer* imaging to identify counterparts, we would have identified 8/9 of the ≥ 3 σ MAMBO galaxies with significant 24 μm sources. Interestingly, all but one of the seven MAMBO sources with robust radio counterparts are detected at 24 μm, the exception being MM J105207.2+572558. Combining the two identification schemes increases our confidence in the identification of the proposed counterparts in both wave bands and provides reliable identifications for *all* nine SMGs in this region.

Detections at 24 μm (FWHM $\sim 6''$) halve the millimeter positional uncertainties (to $\pm 2''$, 95% confidence), although

[11] Dannerbauer et al. (2004) relied on a 1.4 GHz image containing several stripe-inducing >60 mJy sources, with 2–3 times the noise level of the data utilized here. Using equivalent data, our fraction of radio-detected MAMBO sources would fall to 5/9 (34%–75% at ± 1 σ), consistent with Dannerbauer et al. (2004).

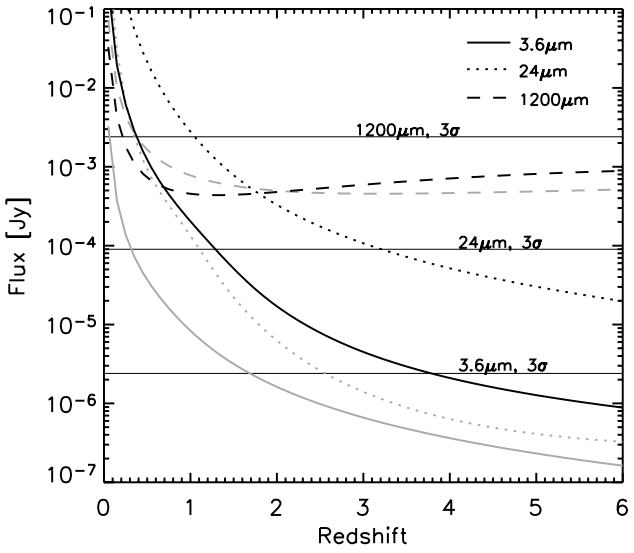

FIG. 2.—Variation of flux density with redshift for Arp 220 (*light lines*) and the active galaxy Mrk 231 (*heavy lines*). Three bands are shown: 3.6, 24, and 1200 μm, together with the 3 σ detection thresholds for our MIR/millimeter observations. As can be seen, our MIR observations are sufficiently sensitive to identify galaxies with luminosities and SEDs similar to either Arp 220 or Mrk 231 out to $z \gtrsim 1$–3. We assume a cosmology with $\Omega_m = 0.3$, $\Omega_\Lambda = 0.7$, and $H_0 = 70$ km s^{-1} Mpc^{-1}. [*See the electronic edition of the Journal for a color version of this figure.*]

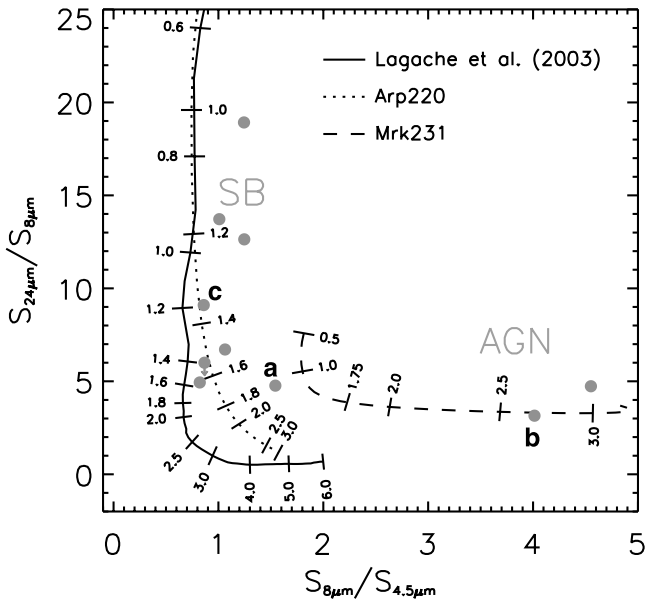

FIG. 3.—Diagnostic color-color diagram showing $S_{24\,\mu m}/S_{8\,\mu m}$ vs. $S_{8\,\mu m}/S_{4.5\,\mu m}$. Tracks for Arp 220 (*dotted line*), a 10^{13} $L_\odot$ synthetic starburst (*solid line*), and Mrk 231 (an active galaxy; *dashed line*) illustrate how these ratios vary as they are moved from $z \sim 0$ to $z \gtrsim 3$. The diagnostic power of this plot lies in the change in slope of the SED at rest-frame ~3–4 μm observed in the spectrum of starbursts. For a submillimeter/millimeter galaxy at $z \sim 2.5$, this results in a pivot around the 8 μm IRAC wave band. Because of their power-law MIR continua, AGNs at $z \geq 1$ typically show higher $S_{8\,\mu m}/S_{4.5\,\mu m}$ at fixed $S_{24\,\mu m}/S_{8\,\mu m}$ than starbursts, providing a simple test of the power source. We chose 4.5 μm for the short-wavelength band because it "comes free" with 8 μm IRAC data; 3.6 μm would work equally well. MIR data for the nine detected MAMBO sources are plotted as points, with the three components of MM J105200.2+572421.9 plotted separately (*a, b,* and *c*). These illustrate how the active galaxies are separated from the starbursts. In theory, some degree of redshift discrimination is also possible via this diagram (see § 4). [*See the electronic edition of the Journal for a color version of this figure.*]

the accuracy remains short of that provided by radio imaging (±0.″6–1.″6, 95% confidence; Ivison et al. 2002). Hence, the radio remains the most useful wave band for localizing the far-IR emission given sufficiently long integrations.

4. WEEDING OUT AGNS

We next investigate the power of MIR observations to identify AGNs within the SMG population. Only one of our nine MAMBO sources has an X-ray counterpart, MM J105200.2+572425 (LE 850.08), previously identified by Ivison et al. (2002). It could be argued that the complexity of this immense merger (there are at least seven distinct optical components in Fig. 4) is such that it would be surprising if at least one of the galaxies were not active! In the absence of the X-ray detection, could we have identified which components contain buried AGNs using only the MIR data? We could. We list the fluxes of the three resolved MIR components in this system separately in Table 1. Figure 1 shows the individual SEDs, arbitrarily placed at $z = 2.5$. The component near-coincident with the brightest *XMM-Newton* and radio emission (*b* in Fig. 4) has a power-law MIR spectrum reminiscent of Mrk 231. Component *a* (previously assumed to be the source of X-rays, based on a less precise centroid from *ROSAT*) was identified as an AGN at $z = 0.97$ by Lehmann et al. (2001), and shows a weak break in slope at an observed wavelength ~4 μm, suggesting a mix of AGN and star formation. Component *c*, on the other hand, has a strong short-wavelength upturn indicative of a starburst. This system allows us to demonstrate the diagnostic power of Figure 3, with component *b* lying close to the track of Mrk 231, well separated from the starburst track; component *a* lies between the AGN and starburst tracks and within $\Delta z \lesssim 0.1$ of its predicted redshift based on the SED of Mrk 231; component *c* is classified as a pure starburst. The main area of possible confusion with this diagram is separating high-redshift starbursts from low-redshift AGNs; fortunately, as in this case, we can expect AGNs at $z \sim 1$ to reveal themselves in other wave bands. On the basis of these tests, it seems reasonable to expect that *Spitzer* will be able to weed out active galaxies within the SMG population.

The MIR data for the other SMGs shown in Figures 1 and 3 display a range of characteristics between the extremes of the Arp 220 and Mrk 231 templates, although the dispersion in Figure 1 must be due partially to the spread in redshift. Over half of the sample display an Arp 220–like upturn in the MIR, with a flat SED out to 8 μm in the observed frame and a sharp rise thereafter, showing that active galaxies, although present, do not dominate the MAMBO population. This is consistent with conclusions drawn from UV/optical spectra and X-ray imaging (Chapman et al. 2003; Alexander et al. 2003). Using the model/empirical tracks to classify the eight MAMBO galaxies with measured 3.6–24 μm SEDs, Figure 3 would indicate six starbursts and two AGNs. Thus, ~75% of the SMGs in our small sample have MIR colors characteristic of high-redshift obscured starbursts. Their MIR colors suggest a median redshift of ~1.4 for our MAMBO sample, somewhat lower than the $z = 2.5$ measured for the radio-detected SMGs of Chapman et al. (2003). This may reflect differences in the selection functions at 850 and 1200 μm, with the latter selecting a somewhat colder, lower redshift and intrinsically lower luminosity section of the population, or it may simply be the result of adopting inappropriate SED templates.

If we assume the MAMBO sources lie at similar redshifts to the SCUBA population and place the MAMBO sources at $z \sim 2.5$, then 8.0 μm corresponds to rest-frame K. It is therefore instructive to compare the MAMBO galaxies with the K-corrected spectrum of Arp 220 (Fig. 3). Arp 220 has an absolute K' magnitude of -24.4, roughly 1.3 L^* (Kim et al. 2002), and would have an 8.0 μm flux of $\sim$2 μJy at $z = 2.5$. The median 8.0 μm flux of the $\geq$4 σ MAMBO sources is $\sim$20 μJy, implying naively that these galaxies are already $\sim$15 L^*. The more plausible alternatives are that these galaxies lie at lower redshifts than we have assumed ($z \sim 1$–2, as implied by Fig. 3) or that their observed 8.0 μm luminosity is dominated by massive, young stars or hot dust. Determining the exact cause of the apparently immense MIR luminosities of these SMGs will require spectroscopic observations in the optical and MIR to confirm their redshifts and the details of their MIR spectral properties.

5. CONCLUDING REMARKS

Spitzer observations between 3.6 and 24 μm of nine galaxies selected at 1200 μm have improved our confidence in the identification of secure counterparts, complementing what was learned from radio imaging. Robust identifications have been possible for $\sim$90% of the MAMBO galaxies using 24 μm imaging, a similar fraction to that achievable from radio imaging. Together, radio and MIR imaging have yielded plausible counterparts for the entire MAMBO sample in this region. We conclude that 3.6–24 μm observations provide a useful tool to aid in identifying SMGs.

Accretion onto an obscured central engine is sometimes betrayed by the shape of the MIR continuum, confirming *Spitzer*'s potential to weed out active galaxies. The fraction of millimeter galaxies with energetically important AGNs in our small sample, 25% (or 9%–49% at ± 1 σ), is similar to that estimated from UV/optical spectroscopy and deep X-ray imaging (Chapman et al. 2003; Alexander et al. 2003), but the majority of MAMBO galaxies have rest-frame mid/far-IR SEDs commensurate with obscured starbursts.

This work is based in part on observations made with the *Spitzer Space Telescope*, which is operated by the Jet Propulsion Laboratory (JPL), California Institute of Technology (Caltech), under NASA contract 1407. Support for this work was provided by NASA through contract 960785 issued by JPL/Caltech.

REFERENCES

Alexander, D. M., et al. 2003, AJ, 125, 383
Bertoldi, F., et al. 2000, A&A, 360, 92
Blain, A. W., Chapman, S. C., Smail, I., & Ivison, R. J. 2004a, ApJ, 611, 725
———. 2004b, ApJ, 611, 52
Blain, A. W., Kneib, J.-P., Ivison, R. J., & Smail, I. 1999, ApJ, 512, L87
Chapman, S. C., Blain, A. W., Ivison, R. J., & Smail, I. 2003, Nature, 422, 695
Cowie, L. L., Barger, A. J., & Kneib, J.-P. 2002, AJ, 123, 2197
Dannerbauer, H., Lehnert, M. D., Lutz, D., Tacconi, L., Bertoldi, F., Carilli, C., Genzel, R., & Menten, K. M. 2004, ApJ, 606, 664
Dunne, L., Eales, S., Ivison, R., Morgan, H., & Edmunds, M. 2003, Nature, 424, 285
Eales, S. A., Bertoldi, F., Ivison, R. J., Carilli, C. L., Dunne, L., & Owen, F. N. 2003, MNRAS, 344, 169
Fazio, G. G., et al. 2004, ApJS, 154, 10
Frayer, D. T., Ivison, R. J., Scoville, N. Z., Evans, A. S., Yun, M., Smail, I., Blain, A. W., & Kneib, J.-P. 1998, ApJ, 506, L7
Genzel, R., Baker, A. J., Tacconi, L. J., Lutz, D., Cox, P., Guilloteau, S., & Omont, A. 2003, ApJ, 584, 633
Genzel, R., & Cesarsky, C. J. 2000, ARA&A, 38, 761
Greve, T. R., et al. 2004, MNRAS, submitted (astro-ph/0405361)
Holland, W. S., et al. 1999, MNRAS, 303, 659
Huang, J.-S., et al. 2004, ApJS, 154, 44
Hughes, D. H., et al. 1998, Nature, 394, 241
Ivison, R. J., Smail, I., Barger, A., Kneib, J.-P., Blain, A. W., Owen, F. N., Kerr, T. H., & Cowie, L. L. 2000, MNRAS, 315, 209
Ivison, R. J., Smail, I., Le Borgne, J.-F., Blain, A. W., Kneib, J.-P., Bézecourt, J., Kerr, T. H., & Davies, J. K. 1998, MNRAS, 298, 583
Ivison, R. J., et al. 2002, MNRAS, 337, 1
Kim, D.-S., Veilleux, S., & Sanders, D. B. 2002, ApJS, 143, 277
Lagache, G., Dole, H., & Puget, J.-L. 2003, MNRAS, 338, 555
Le Floc'h, E., et al. 2004, ApJS, 154, 170
Lehmann, I., et al. 2001, A&A, 371, 833
Neri, R., et al. 2003, ApJ, 597, L113
Omont, A., Petitjean, P., Guilloteau, S., McMahon, R. G., Solomon, P. M., & Pecontal, E. 1996, Nature, 382, 428
Papadopoulos, P. P., Röttgering, H. J. A., van der Werf, P. P., Guilloteau, S., Omont, A., van Breugel, W. J. M., & Tilanus, R. P. J. 2000, ApJ, 528, 626
Rieke, G. H., et al. 2004, ApJS, 154, 25
Rigopoulou, D., Kunze, D., Lutz, D., Genzel, R., & Moorwood, A. F. M. 2002, A&A, 389, 374
Scott, S. E., et al. 2002, MNRAS, 331, 817
Smail, I., Ivison, R. J., & Blain, A. W. 1997, ApJ, 490, L5
Smail, I., Ivison, R. J., Blain, A. W., & Kneib J.-P. 2002, MNRAS, 331, 495
Stevens, J. A., et al. 2003, Nature, 425, 264
Webb, T. M. A., et al. 2003, ApJ, 587, 41
Werner, M. W., et al. 2004, ApJS, 154, 1

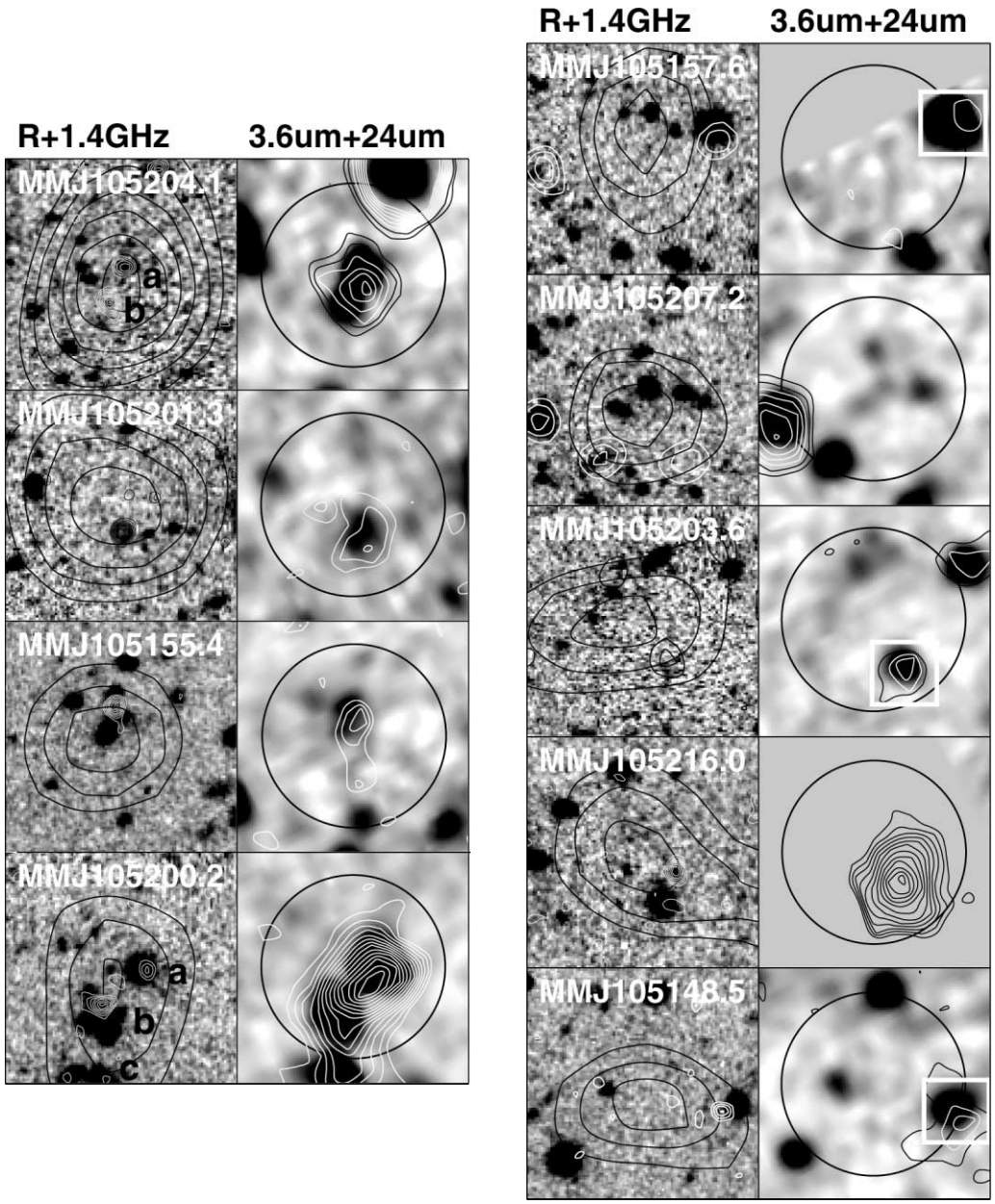

FIG. 4.—Multiwavelength images of $20'' \times 20''$ regions centered on the nine MAMBO sources within the *Spitzer* field. For each source we show (*left-hand panels*) an *R*-band gray scale image with 1200 μm contours overlaid at arbitrary levels and, at finer resolution, 1.4 GHz contours at 2, 3, 4, 5, and 6 σ, where $\sigma = 5$ μJy beam^{-1}; and (*right-hand panels*) a 3.6 μm gray scale image with 24 μm contours (at 3, 4, 5, 6, and 7 σ), where the 3.6 and 24 μm images have been aligned. MAMBO sources are marked by $8''$ diameter circles in the right-hand panels. White squares mark tentative identifications based on weak radio emission near coincident with 24 μm emission.